DEFORMED WING SHAPE PREDICTION USING FIBER OPTIC STRAIN DATA – IFASD 2017

Yang Meng [1], Changchuan Xie [1], and Zhiqiang Wan [1]

[1] Key Laboratory of Aircraft Advanced Design Technology, Ministry of industry and Information Technology
School of Aeronautic Science and Engineering
Beihang University
summy@buaa.edu.cn

Keywords: shape prediction, fiber Bragg grating (FBG) sensors, strain-displacement transformation (SDT), large deformation

Abstract: This study presents a wing shape prediction technique for high-aspect-ratio wings based on measured strains at multiple sensing stations. For the measurement of strain data, fiber Bragg grating (FBG) sensors are used due to their lightness and excellent multiplexing capability. The strain-displacement transformation (SDT) is formulated based on the curvature function of nonlinear beam. The deformed shape is evaluated by numerical double integration of curvature functions. In the laboratory, the developed technique is applied to a high-aspect-ratio wing in which FBG sensors are attached to the surface of the wing beam. The bending deflections are calculated using the proposed method when the wing is subjected to different static loads. At the same time, finite element analysis (FEA) and a laser displacement sensor (LDS) capture the deflection of the wing to validate the estimated wing shape. For three static loading cases, the estimated results obtained by SDT show good agreements with the reference measurements.

1 INTRODUCTION

High-altitude long-endurance (HALE) unmanned aircraft vehicles (UAV) today must be ultralightweight and designed with high aspect ratio and flexible control surfaces. Because of a long wingspan, wings of these aircrafts will undergo large deformations during normal flight, with wingtip displacement reaching to more than 15% of semispan. Thus, the wingtip displacement is a significant parameter for judging the structure status during flight. Besides, it is also a main focus in static aeroelastic analysis. Future HALE aircrafts will require accurate shape sensing to enable multi-functional structural applications and serves for real-time structural health monitoring.

In last decades, various sensing technologies have been developed in measuring the structural deformation. One method is the electro-optical flight deflection measurement system, which is composed of onboard cameras and several explicit targets. This system provides wing displacement information during flight but is too heavy for lightweight wing application. The other one is to determine the structural deformation based on the strain-displacement mapping relationship. The local strains are collected by lightweight and highly multiplexed fiber optic sensors instead of conventional strain gages, which are too heavy and impractical for in-flight wing shape prediction. Using strain data, the structural deformation can be determined by modal analysis [1]. This method is based on strain measurements and strain shape functions,

similar to a Rayleigh-Rize type analysis. Parameters that best fit the measured strain can be used to create a strain-displacement mapping matrix through modal analysis [2-3]. However, this approach is limited in solving a linear problem and requires detailed prior knowledge of boundary conditions and accurate construction of the strain shape functions which can be challenging for complex structures.

Besides the modal method, William L. Ko [4-7] and his coworkers derived a series of displacement equations (called KO theory in NASA) expressed in terms of strains measured at multiple sensing stations equally spaced on the surface of the wing spar. Fiber optic sensors are used to obtain the strain measurements. The KO theory is a numerical algorithm, which is quite simple and efficient, that calculate the displacements by double integration of curvature functions. The main challenge is to expand this method in recovering the large deformation of very flexible wings. In the formulation of the Ko displacement theory, the distribution of bending strains along the discretized cantilever beam was assumed to be piecewise linear. Therefore, the strain curves associated with this theory are the piecewise linear approximations (connecting the strain data points at the strain-sensing stations with straight lines) of the smooth strain curves. These approximations may lose some accuracy locally. Besides, in calculating the wing displacement, the first strain station must have strain data available and a known displacement and slope over the wing's range of motion. In general, the wing root always has a zero displacement and slope, and is typically chosen for the first strain station. However, for the ground test in current work, the fibers did not extend and no strain gage was installed there either. In this study, some modifications will address these drawbacks in Ko displacement theory.

The primary purpose of this paper is to develop a wing shape prediction technique for high-aspect-ratio wings based on measured strains at multiple sensing stations. The double integration method is established and applied to a wing model. Compared to the KO theory, the relation among strain, slope and deflection is reconstructed to deal with the large deformation situation in current work. A finite element model of the wing beam is created and analyzed to validate this method. At the same time, a laser displacement sensor (LDS) directly captures the bending deflections of the wing to validate the estimated wing shape. The estimated results show excellent agreements with the FEA results and reference measurements.

2 THEORETICAL BACKGROUND

2.1 Fiber Optic Sensing Technology

In this work, Fiber Bragg Grating (FBG) sensors are embedding in wing structures for measuring the strains. FBGs are created by exposing an optical fiber to an ultraviolet interference pattern, which produces a periodic change in the core index of refraction [8]. These periodic changes cause a reflection when the light in the waveguide is of a particular wavelength while other wavelengths are transmitted in the optic fiber. The particular wavelength, named Bragg wavelength (λ_B), is determined by the FBG's period of core index modulation (Λ) and the effective core index of refraction (n_0), as expressed in equation (1).

$$\lambda_B = 2n_0\Lambda \tag{1}$$

When the fiber is stretched or contacted, Λ and n_0 increase or decrease, causing a variation in λ_B as represented in equation (2).

$$\delta\lambda_B = 2(\delta n_0)\Lambda + 2n_0(\delta\Lambda) \tag{2}$$

Both strain and temperature can cause changes in n_0 and Λ related to Bragg wavelength. Assuming that the fiber is optically isotropic, the relationship between change in λ_B and strain can be expressed as,

$$\frac{\delta\lambda_B}{\lambda_B} = (1-p_e)\varepsilon + (\alpha_\Lambda + \alpha_n)\Delta T \tag{3}$$

where $\delta\lambda_B$ is the change in Bragg wavelength, λ_B is the unstrained Bragg wavelength, p_e is the strain-optic coefficient, ε is the strain along the fiber-grating-axis direction, α_Λ is the coefficient of thermal expansion of the fiber, α_n is the thermal-optic coefficient. If the experimental environment can be taken as isothermal, the structure strain, ε , is expressed as:

$$\varepsilon = \frac{\delta\lambda_B}{(1-p_e)\lambda_B} \tag{4}$$

2.2 Strain-Displacement Transformation (SDT)

In structural dynamic and aeroelastic analysis of flexible aircrafts, the slender wings of these aircrafts can be modeled as beams by taking advantage of the structure slenderness. A uniform cantilever beam subjected to a tip load is shown in Figure 1.

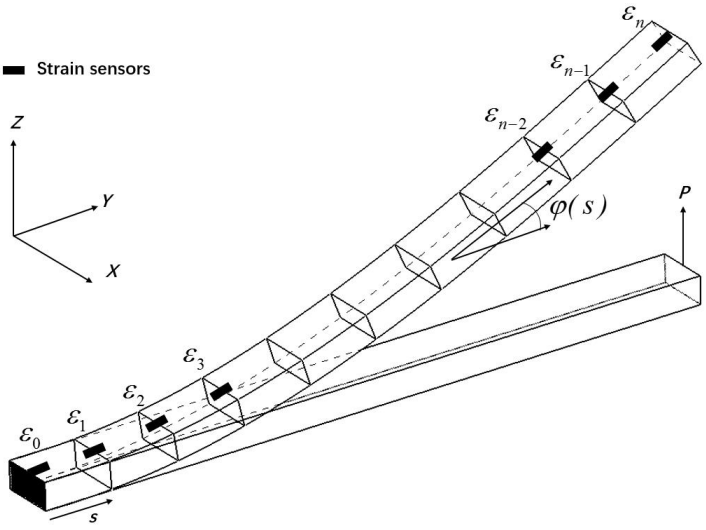

Figure 1: A uniform cantilever beam subjected to a tip load

The origin of the global coordinate system is in the root of the beam (black area in Figure 1). The *X*, *Y* and *Z* axes are defined as edgewise, spanwise and flatwise directions, respectively. Let $\{X(s), Y(s), Z(s)\}$ represent the deformed configuration of the beam, where $S \in [0, L] \subset R$ denotes the coordinate along the centroids of the beam. In this study, the main

focus is to calculate the bending deflection in the Y-Z plane. We designate the tangent angle to the beam curve by φ and write $cos\varphi(s)=Y'(s)$ and $sin\varphi(s)=Z'(s)$, where primes indicate differentiation with respect to *s*. It can be noted that φ is also the rotation angle between the normal to the beam reference line and the *Y*-axis. Therefore, the displacements in the Y-direction and Z-direction can be calculated by equation (5).

$$\begin{cases} Y(\mathrm{s})=\int_0^s cos\varphi(s)\,ds+Y(0) \\ Z(\mathrm{s})=\int_0^s sin\varphi(s)\,ds+Z(0) \end{cases} \tag{5}$$

If the tangent angles are known and the boundary conditions are determined, the deformed shaped can be estimated by this equation. According to ref. [9], the actual bending strain displacement relation is:

$$\kappa=\varphi'-\varphi_0' \tag{6}$$

where κ is the bending strain or curvature function, and φ_0 is the rotation angle of the undeformed beam. Assuming that the undeformed beam is straight ($\varphi_0'=0$) and the bending strain is known. The rotation angles can be calculated by integration of curvature function over $[0,s]$.

$$\varphi(s)=\int_0^s \kappa(s)ds+\kappa(0) \tag{7}$$

In this way, the key to estimate the deformation is to determine the bending strain. The relation between the curvature and the strain of structural surfaces can be represented as:

$$\kappa(s)=\frac{\varepsilon(s)}{c(s)} \tag{8}$$

In equation (7), ε is the strain that can be measured by strain sensors installed on the structural surface, and c is the distance between the sensing position and neutral axis location (for a uniform beam, *c* is the beam half depth). As shown in Figure 1, a set of strain values $\{\varepsilon_0,\varepsilon_1,\ldots,\varepsilon_n\}$ can be obtained by fiber optic sensors at certain sensing stations $\{s_0,s_1,\ldots,s_n\}$, which satisfy the relation: $0=s_0<s_1<\ldots<s_n=L$. Strain values at the domains can be determined by cube interpolation using these measured strains. Due to the limitation of sensors installation, ε_0 is usually not available in experiment. Interpolation is not possible at the root of the test article. Therefore, the strain values near to the root are extrapolated. To keep the accuracy of the extrapolation, the fiber optic sensor is installed as close to the root as possible. For the purpose of this paper, the order of the polynomial curve fit was not formally optimized.

After the strain values at different positions are obtained, the rotation angles and the displacements can be calculated by numerical integration. The detailed numerical calculations are not presented in this paper.

3 EXPERIMENTAL DESIGN

3.1 Wing model

A beamlike metallic wing was designed. Its detail parameters are listed in Table 1, and its shape could be seen in Figure 2. The model consists of two parts: rectangular wing and weighting tube on the wing tip. The stiffness of the wing is mainly supplied by a steel beam. The aspect ratio of this wing model is 10. There are 8 wood-made wing boxes and the gap between the boxes is about 3mm. NACA0015 airfoil was adopted and the material of the skin is tissue paper. The wingtip weighting tube is designed to adjust the torsional mode by changing the torsional moment of inertia. Its length is 190mm. The front and real cone are made of steel, and the middle part is made of aluminum.

Overall parameters		Weighting tube		Wing beam	
Span(*mm*)	1000	Material	Aluminum	Material	Steel
Chord(*mm*)	100	Length(*mm*)	190	Width(*mm*)	35
Airfoil	NACA0015	Weight(*g*)	60	Thickness(*mm*)	1.5
Elastic axis	50% chord	Diameter(*mm*)	10.9		
Total mass(*g*)	672				

Table 1: Parameters of the wing model

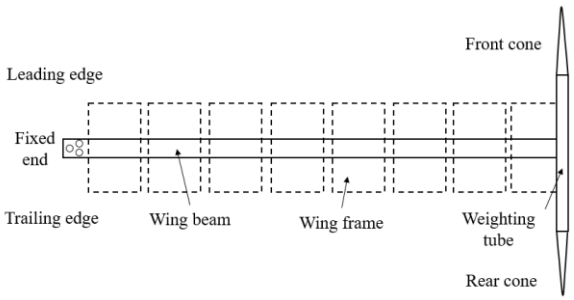

Figure 2: The beamlike wing model

In ground vibration test, the wing beam was fixed vertically to eliminate the nonlinear effect induced by large deformation under gravity. The tested model can be seen in Figure 3. The test results are listed in Table 2, in which the analysis results of linear vibration are also listed for comparison. Finite element analysis(FEA) results are obtained by NASTRAN SOL103.

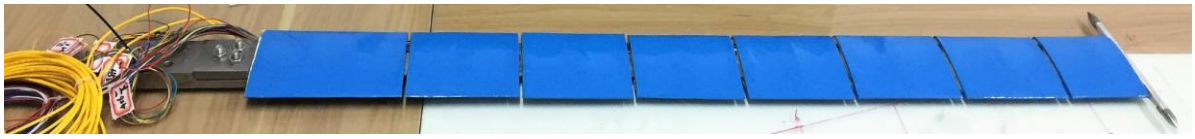

Figure 3: The wing model for ground test

Mode	Description	f_{exp}, Hz	f_{FEA}, Hz	Error, %
1	First flat bend	1.14	1.141	0.08
2	Second flat bend	7.58	7.474	1.4
3	First torsion	22.17	22.92	3.38

Table 2: Natural modes and frequencies of the wing model

3.2 Sensor arrangement

Figure 4 shows the wing beam with locations of ten embedded FBG sensors. These sensors are divided into two groups, each of which contains five sensors with different Bragg wavelength. The five sensors were manufactured and multiplexed in a single optical fiber. Two channel are needed for collecting data from the sensors. Epoxy adhesive is used to attach the optic fiber with sensors to the structural surface. The origin of the global coordinate system is at the root of the wing model. The *X*, *Y*, *Z* axes are defined as edgewise, spanwise and flatwise directions, as shown in Figure 4. The two sensing lines are parallel to the *Y* axis, and the distance between them is 27mm. Positions of these ten sensors along Y axis are listed in Table 3. The sensor directions were set to 0° along the spanwise direction (*Y*-axis of the global coordinate).

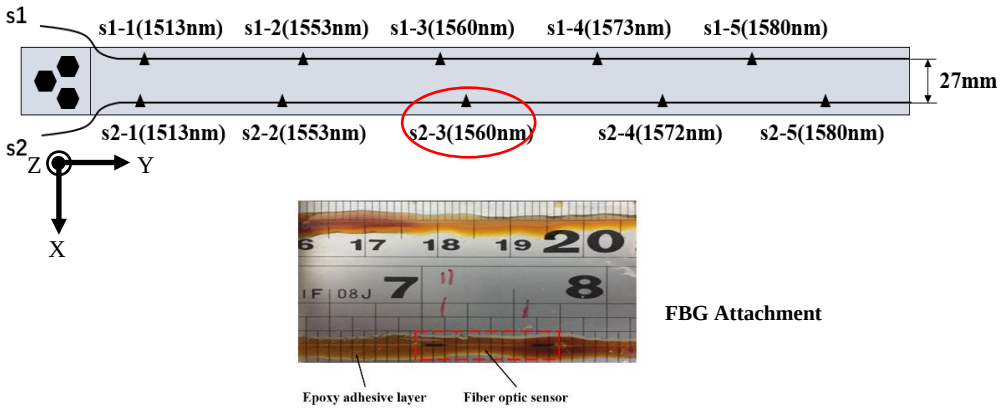

Figure 4: Locations of FBG sensors with node number and wavelength of each sensor and the way of attaching to structure surface.

Node number	Position(mm)	Node number	Position(mm)
s1-1	54	s2-1	40
s1-2	246	s2-2	240
s1-3	413	s2-3	450
s1-4	565	s2-4	650
s1-5	754	s2-5	900

Table 3: Locations of FBG sensors

3.3 Test setup and test cases

The shape estimation technique was validated from static tests of the designed wing model. The strains were measured when the flexible wing was subjected to gravity and certain tip loads. The entire test setup is depicted in Figure 5. The wing model was installed on the test jig. The attached FBG sensors were connected to an FBG interrogator (sm130, Micron Optics Inc., USA) with FBG ingress/egress ports. A laser displacement sensor was used to capture

the vertical displacements at eight different positions including the wing tip. In current work, the main focus is to predict the flatwise bending deformation of the wing model. The edgewise bending and torsional deformation are not considered here. Thus, three load conditions that produce vertical bending deflection in the Y-Z plane were employed in the static tests as listed in Table 4. Since there is little difference of the strain data between fiber s1 and s2, we chose those measured by FBG sensors in fiber s1 as the measurands.

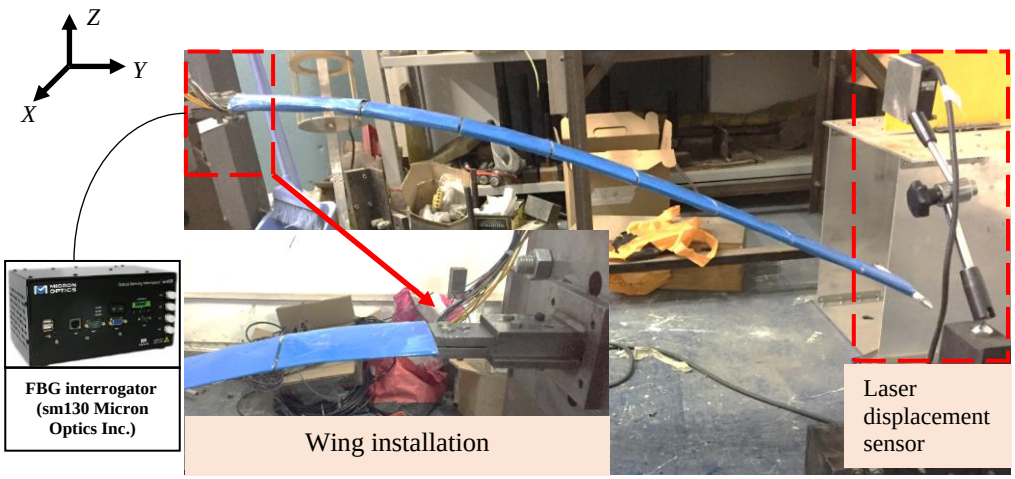

Figure 5: Experiments setup for wing shape prediction test. The wing is fixed horizontally, and deforms under gravity and certain tip loads. Laser displacement sensor was used to capture the vertical displacements.

Cases	Measurands	Description
1	Wavelengths of five FBG sensors of s1; Displacements captured by LDS	Under gravity
2		Under gravity and a tip load along the Z-axis: P_1=-0.584N
3		Under gravity and a tip load along the Z-axis: P_2=-0.971N

Table 4: Test cases and measurands

4 RESULTS AND ANALYSIS

The strain data collected from the qualification wing model subjected to gravity load is plotted along with the corresponding FEA results in Figure 6. The squares represent the experimental data measured by fiber optic sensors, the solid line represents the fitting results of the strains, and the dash line represents the FEA results. Because the upper surface of the wing beam is stretched under gravity, the strain values are positive. It can be seen that the strain curve is not a straight line but a slightly bent curve. The largest percentage difference is 3.85% in the wing root. It shows that the accuracy of the extrapolation of strain data is acceptable. The experimental data and the FEA results show very good agreements.

Figure 7 shows the wing deflection curves under gravity load, calculated from deflection equation (7), using the strain data at the strain-sensing stations. For comparison, the deflections calculated from FEA (dash line) and captured by LDS (dash dot line with close triangular symbols) are also plotted in Figure 7. The SDT results and FEA results show a good agreement in both spanwise displacements and bending displacements. It can be seen that there is no spanwise displacements in the deflection curve obtained by LDS. From the LDS results under gravity load condition, the wingtip bending deflection is up to 0.34m, which is 34% of the wing span. The largest percentage differences in displacements occur in the wing tip. For the gravity load condition, the difference between the FEA results and SDT

is 7.14% in the Y-direction. Keep in mind that the absolute values of the spanwise displacements are quite small, the difference percentage is acceptable. The difference between the LDS results and the FEA results is 1.03% in the Z-direction, and the difference between the LDS results and the SDT results is -2.43% in the Z-direction. The absolute value of the latter one is larger than the former one. Both of the differences in Z-direction are less than 5%. The excellent agreement between the three sets of deflection curves shows the high accuracy of the double integration of bending strains for the tested wing model. Detailed information could be found in Table 5.

Cases		Gravity	Gravity and P_1	Gravity and P_2
Spanwise, *Y*	FEA	-0.06785	-0.09257	-0.10906
	SDT	-0.07307	-0.10417	-0.12292
	Difference, %	7.14	11.14	11.28
Bending, *Z*	LDS	-0.34	-0.393	-0.425
	FEA	-0.33651	-0.38906	-0.41963
	Difference, %	1.03	1.0	1.26
	LDS	-0.34	-0.393	-0.425
	SDT	-0.34825	-0.41078	-0.44316
	Difference, %	-2.43	-4.52	4.27

Table 5: Comparison of the wingtip displacements calculated by FEA, SDT with those measured by laser displacement sensors

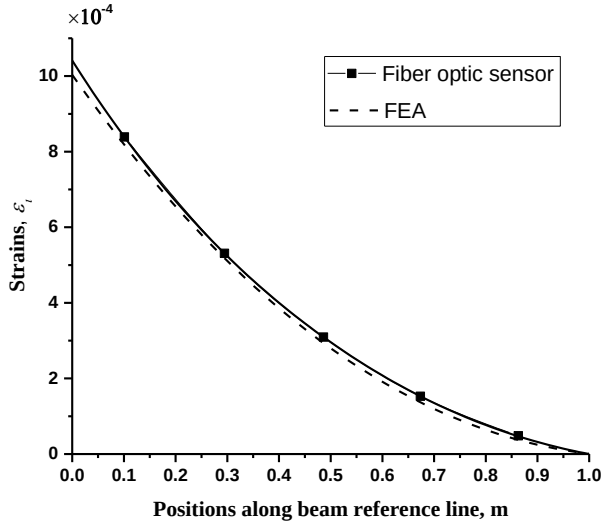

Figure 6: Case1; Comparison of Bending strains, ε_i, at different sensing stations, measured by fiber optic sensors with those calculated by finite element analysis.

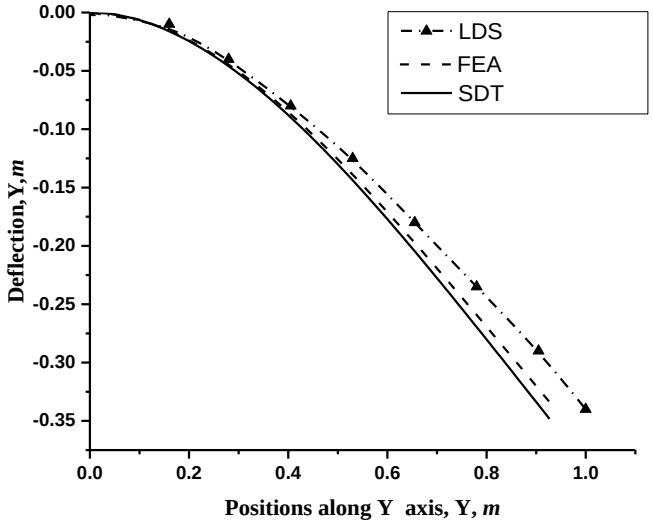

Figure 7: Case1; Comparison of deflections calculated by FEA, SDT with those measured by laser displacement sensors.

Figure 8 and Figure 10 show the strain curve of the wing model subjected to the second and the third load case, respectively. In these cases, the strain curves are deeply bent, not straight lines. Thus, the piecewise linear approximation in Ko theory may lose some accuracy locally in solving these problems. The largest percentage differences are 7.32% in the second case, and 7.52% in the third case, both in the wing root.

Figure 9 and Figure 11 shows the deflection curves of the wing model subjected to the second and the third load case. For these two load cases, the wingtip bending deflection is up to 0.393m (39.3% of the wing span), and 0.425(39.3% of the wing span), respectively. Combined with the results in Table 5, the percentage differences are no more than 5% in Z-direction.

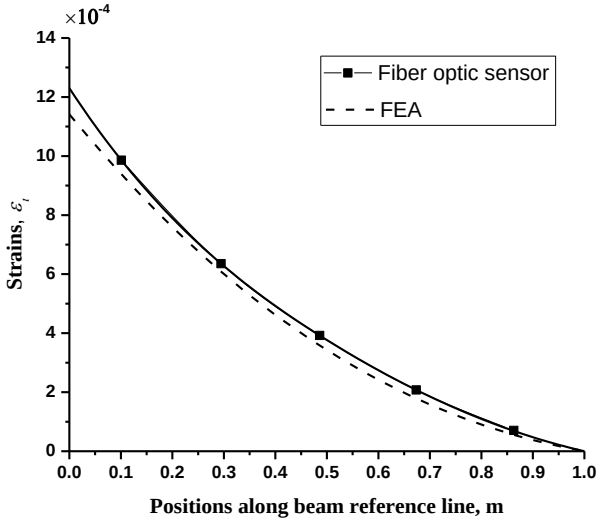

Figure 8: Case2; Comparison of Bending strains, ε_i, at different sensing stations, measured by fiber optic sensors with those calculated by finite element analysis.

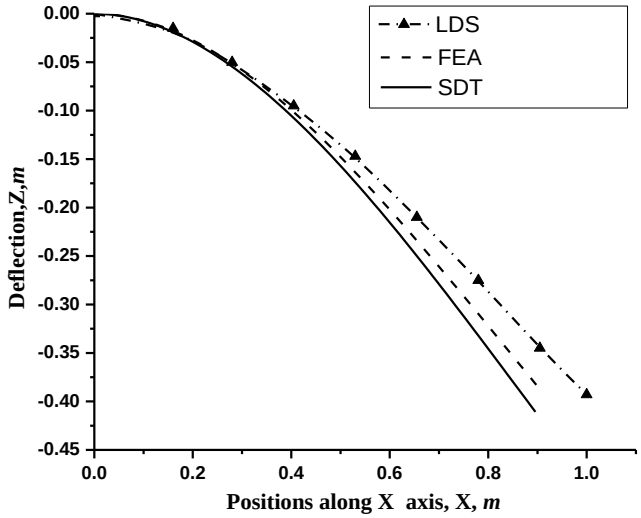

Figure 9: Case2; Comparison of deflections calculated by FEA, SDT with those measured by laser displacement sensors.

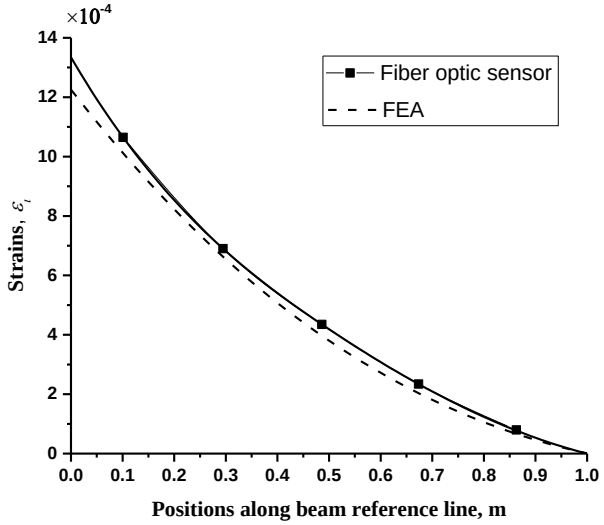

Figure 10: Case3; Comparison of Bending strains, ε_i, at different sensing stations, measured by fiber optic sensors with those calculated by finite element analysis.

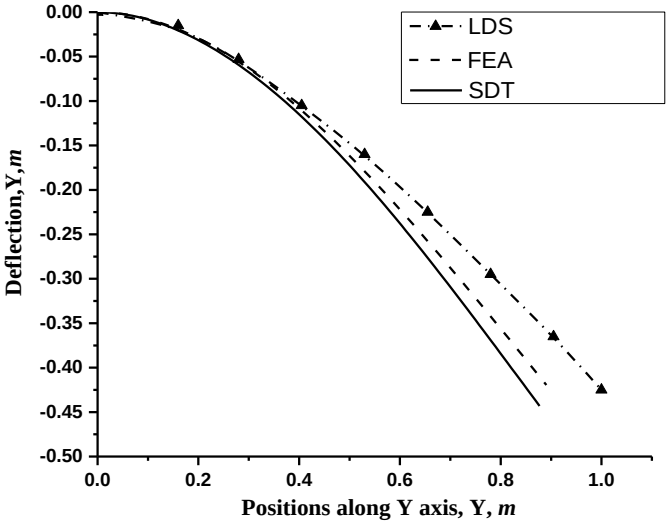

Figure 11: Case3; Comparison of deflections calculated by FEA, SDT with those measured by laser displacement sensors

5 CONCLUSIONS

This paper explored the accuracy of wing shape calculations (bending only), using strain data from fiber optic sensors measurements. The strain data collected from the experiment was compared to a set of analytical FEA results in order to obtain a quick assessment of differences between the experimental data and FEA results. Besides, the bending deflections were calculated by the finite element analysis, strain-displacement transformation using the strain data and captured by the laser displacement sensors, respectively. The principal finds are as follows:

(1) The bending deflections along the spanwise direction were expressed explicitly in terms of geometrical parameters of the wing model and bending strains at all the inboard strain-sensing stations.

(2) The strain data collected from the fiber optic measurements show a good agreement with the FEA results under the same load conditions.

(3) The percentage differences between the LDS results and the SDT results are no more than 5% in Z-direction. The excellent agreement shows the high accuracy of the double integration of bending strains for the tested wing model.

6 REFERENCES

[1] Kim, H., J. Han, and H. Bang," Real-time deformed shape estimation of a wind turbine blade using distributed fiber Bragg grating sensors", WIND ENERGY Vol. 17, 2014, pp. 1455-1467.

[2] Kirby, G. C., Lim, T. W., Weber, R., Bosse, A. B., Povich, C., Fisher, S. Strain-based shape estimation algorithms for a cantilever beam. In Proceedings of SPIE 3041 Smart Structures and Materials (p.788-798), 1997.

[3] Bang, H.-J., Kim, H.-I., Jang, M., & Han, J.-H. Tower deflection monitoring of a wind turbine using an array of fiber Bragg grating sensors. In Proceedings of the ASME 2011 conference on smart materials, adaptive structures and intelligent systems. Scottsdale, Arizona, USA. (SMASIS2011-5033), 2011.

[4] Ko, W.L., W.L. Richards, and Van T. Tran, "Displacement Theories for In-Flight Deformed Shape Predictions of Aerospace Structures", Edwards, California: NASA Dryden Flight Research Center, 2007.

[5] KO, W.L., W.L. Richards, and Van Tran Fleischer, "Applications of KO Displacement Theory to the Deformed Shape Predictions of the Doubly-Tapered Ikhana Wing", Edwards, California: NASA Dryden Flight Research Center, 2009.

[6] Ko, W.L., and Van Tran Fleischer, "Further Development of Ko Displacement Theory for Deformed Shape Predictions of Nonuniform Aerospace Structures", Edwards, California: NASA Dryden Flight Research Center, 2009.

[7] Ko, W.L., and Van Tran Fleischer, "Methods for In-Flight Wing Shape Predictions of Highly Flexible Unmanned Aerial Vehicles Formulation of Ko Displacement Theory", Edwards, California: NASA Dryden Flight Research Center, 2010.

[8] Richards, W.L., A.R. Parker, W.L. Ko, A. Piazza, and P. Chan, "Application of Fiber Optic Instrumentation": Research and Technology Organization, 2012.

[9] Reissner, E.," On One-Dimensional Finite-Strain Beam Theory: the Plane Problem", Journal of Applied Mathematics and Physics Vol. 23, 1972, pp. 795-804.

ACKNOWLEDGEMENT

This work was supported by the National Key Research and Development Program (2016YFB0200703).

COPYRIGHT STATEMENT